Chapter 3 The Polarized ^{3}He Target

The E94-010 experiment used polarized ^{3}He as a source of polarized neutrons. The design was based upon a similar target built at SLAC [50]. Polarization of the ^{3}He nuclei was achieved via spin-exchanged collisions with optically pumped rubidium vapor [51, 52, 53, 54]. Details of this process along with a description of the target design and target cells are covered in this chapter.

3.1 Optical Pumping and Spin Exchange

3.1.1 Optical Pumping

The first step towards polarizing the ^{3}He nucleus is to create a source of polarized electrons that will later collide and transfer their spin polarization to the ^{3}He nuclei. These polarized electrons are provided by optically pumping Rb atoms. A review of optical pumping of alkali metals is described by W. Happer [51] and more recently by S. Appelt *et al.* [55]. Rubidium has a single outer shell electron ($5S_{1/2}$) and when placed in a magnetic field its Hamiltonian operator is given by [55]

$$\hat{H}_g = A_g \hat{\mathbf{I}} \cdot \hat{\mathbf{S}} + g\mu_B \hat{S}_z B_z - \frac{\mu_I}{I} \hat{I}_z B_z. \tag{3.1}$$

The first term of Equation 3.1 represents the vector coupling of the electron's spin ($\hat{\mathbf{S}}$) to the spin of the nucleus ($\hat{\mathbf{I}}$), with a strength given by A_g. The last two terms of Equation 3.1 describe the coupling of the electron and nuclear spins to the magnetic field (B_z). The strength of these couplings is proportional to the value of the magnetic field and depends on the g value for the electron (g=2.00232), the Bohr magneton (μ_B=9.2741$\times$10^{-21} erg G^{-1}), the nuclear magnetic moment (μ_I) in nuclear magnetons, and the nuclear-spin quantum number ($I = 5/2$ for ^{85}Rb and $I = 3/2$ for ^{87}Rb). The electron is an eigenstate of the total spin quantum number $F = I + S$, which equals 3 or 2 for ^{85}Rb (76.6% natural abundance) and 2 or 1 for ^{87}Rb (23.4% natural abundance). The presence of a magnetic field splits the F state into various sub-levels: m_F.

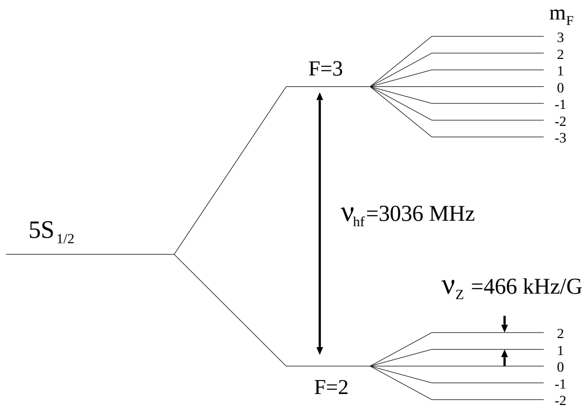

Figure 3.1: Level diagram for ^{85}Rb. The Zeeman splitting of the m_F sub-levels is given by ν_Z.

The process of optical pumping begins by exposing a sample of rubidium vapor with circularly polarized photons tuned to the D1 ($5S_{1/2} \longrightarrow 5P_{1/2}$) transition. If the photon helicity is in the same direction as the magnetic field, then electrons from all sub-levels, except the $m_F = 3$ (for the case of ^{85}Rb) sub-level, can be excited. These excited electrons can return to any of the ground state sub-levels. In time, all but the $m_F = 3$ sub-level will become depopulated.

A simplified form of the optical pumping process is shown in Figure 3.2. Here electrons in the $m_J = -1/2$ ground state are excited to the $(5P_{1/2}, m_J = 1/2)$ state where they decay to the $m_J = 1/2$ and $m_J = -1/2$ ground states. Since selection rules prohibit the $m_J = 1/2$ ground state electrons from being excited, the $m_J = -1/2$ ground state will quickly become depopulated.

As excited electrons return to the ground state they will emit a photon at the D1 wavelength (795 nm). This photon is randomly polarized and can excite electrons from the $m_F = 3$ ground state. Since optical pumping relies on these electrons not being excited, a method known as quenching is employed to prevent the optical de-excitation of electrons. A buffer gas of N_2 is introduced. Collisions between the Rb and N_2 allow, through the mechanical excitation of N_2, the electron to decay without emitting a photon. The amount of N_2 gas is chosen to be a couple of orders of magnitude less than the ^{3}He density and few orders of magnitude more than the Rb density. For this condition, only about 5% of excited electrons decay by emitting a photon [50].

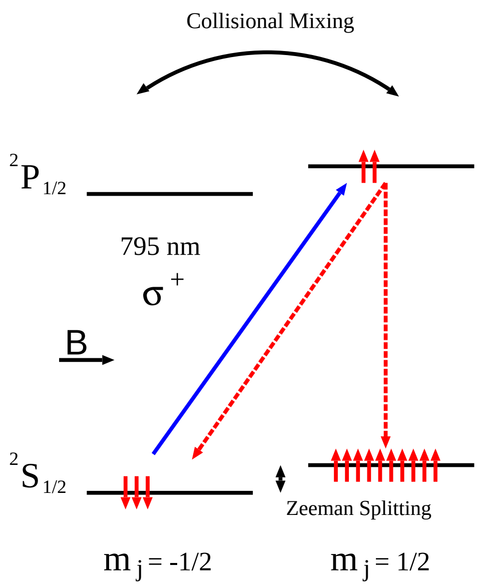

Figure 3.2: Optical pumping of Rubidium.

In regions of abundant laser light, high Rb polarization is expected. The local polarization (P_{Rb}) of the Rb vapor is given in terms of the optical pumping rate (R) and the spin destruction rate (Γ_{SE}):

$$P_{Rb} = \frac{R}{R + \Gamma_{SD}}. \tag{3.2}$$

The electron spin destruction rate is primarily governed by collisions of Rb atoms with other gas particles, as opposed to collisions with the wall or depolarization from photons created by optical de-excitation. The rate is given by:

$$\Gamma_{SD} = k_{Rb-He}[^3He] + k_{Rb-Rb}[Rb] + k_{Rb-N_2}[N_2] \tag{3.3}$$

The spin destruction rate constants, k_{Rb-x}[cm^3/s], have been measured by Wagshul and Chupp [56]: $k_{Rb-He} \leq 2 \times 10^{-18}$, $k_{Rb-Rb} = 8 \times 10^{-13}$, and $k_{Rb-N_2} = 8 \times 10^{-18}$. The densities of the various species for our experiment are [He]$\approx 2\times10^{20}$cm^{-3} and [N_2]$\approx 2\times10^{14}$cm^{-3}; the rubidium density is given by the Killian formula [57]: [Rb] $= 1.507 \times 10^{26}(\frac{10^{-4040/T}}{T}) \approx 2.5 \times 10^{18}$cm^{-3} for $T = 170$°C. An order of magnitude approximation for the spin destruction rate is $1/\Gamma_{SD} = 10^{-3}$s. The depopulation rate of the $m_j = -1/2$ ground state is on the order of 10^{-6}s [53]. Rubidium vapor is therefore nearly 100% polarized in regions where optical absorption is occurring and nearly zero in regions where the light does not penetrate.

3.1.2 Spin Exchange

The transfer of polarization from the Rb electrons to the ^{3}He nuclei occurs through a weak hyperfine interaction in which a ^{3}He nucleus collides and exchanges its spin with the outer electron of rubidium. The evolution of the ^{3}He polarization ($P_{He}(t)$) is given by:

$$P_{He}(t) = < P_{Rb} > \frac{\gamma_{SE}}{\gamma_{SE} + \Gamma}\left(1 - e^{-(\gamma_{SE}+\Gamma)t}\right), \tag{3.4}$$

where $< P_{Rb} >$ is the volume average rubidium polarization, the spin exchange rate is given by $\gamma_{SE}=k_{SE}$[Rb], and Γ is the ^{3}He nuclear spin relaxation rate in the absence of Rb vapor or an electron beam. The spin exchange rate constant was measured to be $k_{SE} = (6.7 \pm 0.6) \times 10^{-20}$[cm^3/s] [52]. For our rubidium density, γ_{SE} is about 1/(10 hrs). The relaxation rate was measured for each cell and had a typical value of about 1/(40 hrs). A typical maximum polarization for the cells out of the electron beam was 40%. Working backwards, this implies a volume averaged Rb polarization of about 60%. Although procedures exist to measure the Rb polarization [58], they were not implemented for this experiment.

3.2 Target Cells

The optical pumping and spin exchange process take place within a target cell. The cells are made from an aluminum-silicate glass (Corning 1720 or GE180) and are comprised of three parts: a pumping chamber, a target chamber, and a transfer tube (Figure 3.3). The pumping chamber is spherical and was placed within a plastic oven in order to control the rubidium vapor density. The target chamber is a 40 cm tube that was placed along the electron beam path. The transfer tube simply connects the two chambers.

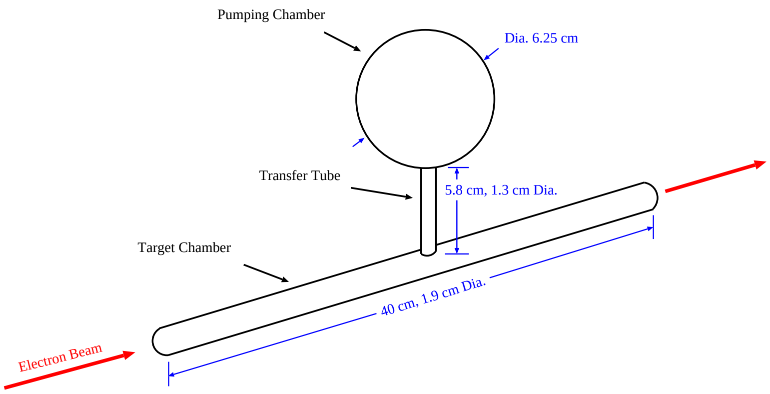

Figure 3.3: A target cell with basic dimensions.

Six target cells were used for this experiment and each cell was given a name: *Don't Worry, Be Happy, Armageddon, Nepheli, Sysiphos,* and *Jin.* Their construction involves three steps. First, stock tubing is blown to a larger diameter for the target chamber and transfer tube. This is done in order to reduce the presence of micro fissures along the interior walls. A spherical cell is formed separately to make the pumping chamber. All three parts are cleaned with an acid wash, joined, and then connected to a glass string that is attached to a vacuum system. The second step is to bake the target cell while under vacuum. This reduces the presence of paramagnetic impurities that cause depolarization via collision with ^{3}He or rubidium. Once the cell is baked out and a good (10^{-9} torr) vacuum is achieved, the cell is filled. First, rubidium is chased into the pumping chamber. Next, N_2 gas is filled into the cell to a pressure of 60-70 torr. Last, the cell is filled to about 10 atm. of ^{3}He. Before the cell is sealed, or "tipped off," a container of liquid helium is placed around the target chamber. This reduces the internal gas pressure to below 1 atm. and makes the target cell safe to tip off.

By studying the decay of polarization in an apparatus similar to the one described in Section 3.3, a cell's lifetime ($=1/\Gamma$) was measured. The lifetime of a cell is the amount of time it takes for the ^{3}He polarization to drop by a factor of $1/e$ when the cell is at room temperature and no electron beam is present. A cell with a short lifetime ($\leq$20 hrs) cannot obtain high polarization. Lifetime was an important selection criterion on cell quality. The lifetimes are listed in Table 3.1.

Cell	Lifetime (hours)
Don't Worry	43.5±1
Be Happy	39.5±1
Armageddon	40±1
Nepheli	20±1
Sysiphos	53±1
Jin	29±1

Table 3.1: Lifetimes for the target cells measured after construction.

3.2.1 Cell Geometry

A cell's mechanical properties are important for accurately determining the amount of ^{3}He polarization, the density of the target as seen by the electron beam, and the amount of material through which the incident and scattered electron pass. The relevant pieces of information needed are: the thickness of the target chamber entrance window, the thickness of the target chamber wall, the total internal volume, the volumes of the three target cell components, and the inner radius of the target chamber. The following sections describe how the cell geometry was characterized.

Window Thickness

The entrance and exit windows for the target chamber were constructed to have thin windows ($\approx$100 microns). Accurate measurement of the window thickness is important in understanding the amount of energy the electron loses as it passes through the glass window for estimating radiative corrections.

Two methods were used to measure the window thickness: one mechanical and the other optical. After the end windows were blown, they were measured using a micrometer of 1.3 μm resolution [50]. The results are listed in Table 3.2 and should only be considered a check of the optical method. The optical method used scattered laser light from the surface of the window. The intensity of the light depends on the wavelength and window thickness. The intensity of reflected light off of a parallel plate is given by [59]:

$$I_r = \frac{\frac{4\left(\frac{n-1}{n+1}\right)^2}{\left(1-\left(\frac{n-1}{n+1}\right)^2\right)^2} \sin^2\left(\frac{2\pi n t \cos\theta_2}{\lambda}\right)}{1 + \frac{4\left(\frac{n-1}{n+1}\right)^2}{\left(1-\left(\frac{n-1}{n+1}\right)^2\right)^2} \sin^2\left(\frac{2\pi n t \cos\theta_2}{\lambda}\right)}, \tag{3.5}$$

where n is the index of refraction (1.528$\pm$0.01), λ is the wavelength of the incident laser light (780 nm), θ_2 is the angle of the refracted light (3.27°), and t is the thickness of the window. The basic setup is shown in Figure 3.4. For the surface to be considered a parallel plate, a small beam spot size was used and only the reflected light that was in the same plane as the incident beam and surface normal was detected. By recording and fitting the variation of the intensity as a function of wavelength to Eq. 3.5, the thickness was determined to an uncertainty of $\pm$0.5%. Results are listed in Table 3.2.

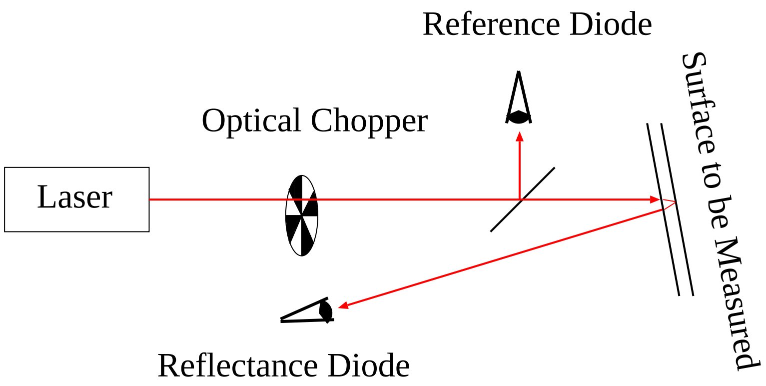

Figure 3.4: Setup for an interferometric thickness measurement.

Internal Volume

The total internal volume can be measured precisely using Archimede's principle, which equates the magnitude of the buoyant force to the weight of the fluid displaced. After a cell was created, it was tied to a block of known volume and weight, attached to a scale, and lowered into a bath of water. The internal volume, $V_{internal}$, of the target cell is given by:

$$V_{internal} = \frac{1}{\rho_g}\left(\rho_b V_b + m_{He} + \rho_g V_w - \rho_g V_b - \rho_w V_w - \frac{W_{c+b}}{g}\right), \tag{3.6}$$

where g is the gravitational constant, ρ_g is the density of glass, ρ_b is the density of the block, ρ_w is the density of water, V_g is the volume of the glass, V_b is the volume of the block, V_w is the volume of the water displaced by the cell-block combination, W_{c+b} is the weight of the cell-block combination when it is submerged, and m_{He} is the estimated mass of the ^{3}He (0.3 grams). The precision of this method is about 0.5% with the dominant uncertainty coming from the measurement of the amount of displaced water. Results are listed in Table 3.3.

Determining the internal volume is the first step towards calculating the volumes of the various chambers. The internal volume of a particular chamber was determined in two ways. The first is done by multiplying a chamber's outer volume by the ratio

Target Cell	Window #	Thickness [μm] Mechanical	Optical
Don't Worry	2	137.2±1.3	135.9±0.6
	21	143.5±1.3	140.1±0.5
Be Happy	4	129.5±1.3	-
	5	132.1±1.3	135.3±1.6
Armageddon	VII	125.7±1.3	121.9±0.6
	XVIII	142.2±1.3	139.1±0.7
Nepheli	-	-	-
	-	-	-
Sysiphos	9	152.4±1.3	134.2±1.0
	18	132.1±1.3	121.0±1.0
Jin	14	142.2±1.3	136.1±1.2
	15	137.2±1.3	134.8±0.8

Table 3.2: Target chamber window thicknesses. *Nepheli*'s windows were not recorded.

Cell	Wall Thickness ave. [mm]	uncertainty	r_{target} [cm]	V_{pump} [cm^3]	$V_{transfer}$ [cm^3]	V_{target} [cm^3]	V_{total} [cm^3]
Don't Worry	0.995	3.7%	0.843	107.7	6.5	82.8	197.1
Be Happy	0.990	9.0%	0.833	122.3	5.1	89.8	217.2
Armageddon	1.182	9.0%	0.810	97.2	4.9	86.4	188.5
Nepheli	0.956	9.0%	0.860	104.2	6.4	91.0	201.5
Sysiphos	0.986	2.5%	0.902	110.0	5.5	97.0	212.4
Jin	0.874	4.0%	0.866	102.0	8.4	89.1	199.5

Table 3.3: Internal dimensions for the target cells.

of the total internal and external volumes:

$$V_{chamber}(internal) = V_{chamber}(external)\frac{V_{internal}}{V_{external}}. \tag{3.7}$$

A caliper was used to measure the external volumes.

A second method starts by using the external dimensions and subtracting away the glass thickness. The amount subtracted was determined using the results of the total internal volume measurement. In this way, internal dimensions were predicted and volumes calculated. Results are listed in Table 3.3. The two methods agreed to within

1%. Taking this into consideration, along with the uncertainty in the total internal volume, a ±1.5% uncertainty was placed on the chamber volume determination.

Target Chamber Wall Thickness

Measurement of the target chamber wall thickness was carried out in the same manner as the window thickness. The measurements were performed after the experiment on the surviving target cells: *Don't Worry, Sysiphos*, and *Jin*. For these cells, the average variation of the thickness (t) along the length of the cell was $\frac{\Delta t}{t} = 0.03$. The uncertainty on the average thickness was about ±3.5%.

For the target cells that did not survive the experiment–*Be Happy*, *Armageddon*, and *Nepheli*–a thickness had to be inferred from a comparison of the optical method to a method which assumes a constant cross-sectional area during the enlarging process. Recall that the stock tubing for the target chamber is blown to a larger diameter to remove micro-fissures. The original stock tubing had an outer radius $r_o = 0.741$ cm for Corning 1720 and 0.788 cm for GE 180 and an inner radius of $r_i = 0.630$ cm for Corning 1720 and $r_i = 0.621$ for GE 180. The thickness is predicted from measuring the resized tube's outer radius (r_o'):

$$thickness = r_o' - \sqrt{(r_o')^2 - (r_o^2 - r_i^2)}. \tag{3.8}$$

The optical method on surviving cells found a systematic shift of 14%±9% greater thickness than the mechanical method. The mechanical thicknesses of *Be Happy*, *Armageddon*, and *Nepheli* were adjusted by adding this amount. Results are listed in Table 3.3.

3.2.2 Cell Density

Knowledge of the ^{3}He density within the target cell was needed for calculating radiative corrections, determining the target polarization, and, eventually, for extracting the ^{3}He total cross section. Two methods were used to measure the ^{3}He density. One relies on keeping track of temperatures, volumes, and pressures during the filling process. The other is an optical technique. Both methods were to find the final density for each target cell.

During the filling process ^{3}He is deposited into the target cell from a calibrated volume (Figure 3.5). The volume is filled with a small amount of ^{3}He to a particular pressure and then released into the target/string combination. By repeating the process, the final desired number density of the ^{3}He is obtained. This "fill density" is calculated from the ideal gas law and is given by [60]:

$$n_0 = \frac{1}{k_B T_{fill} V_{cell}} \left(\left(\sum_{j=1}^{N-1} (P_j^{int} - P_j^{final}) + P_N^{int} \right) V_{fill} - P_{final}(V_{fill} + V_{string-cell}) \right), \tag{3.9}$$

where n_0 is the number density of the ^{3}He within the target cell, N is total number of times the cell is filled from the calibrated volume, P_j^{int} is the pressure in the fill volume after charging it up for the j-th time, P_j^{final} is the equilibrium pressure after opening the valve to the string/target cell for the j-th time, P_{final} is the equilibrium pressure in the charge volume and string after the target cell has been pulled off, T_{fill} and V_{fill} are the temperature and volume of the calibrated volume, and $V_{string-cell}$ is the volume of the string after the cell has been pulled off. Results are listed in Table 3.5. The uncertainty in this method is 2.2%.

Once a cell has been created, its density can be measured by observing the collisional absorption broadening [61, 62]. The natural D1 and D2 absorption lines of Rb are broadened by the presence of ^{3}He. By measuring the absorption spectrum, the density of ^{3}He was determined.

The absorption spectrum has the form $\ln \frac{I(0)}{I(\nu)} \sim \sigma(\nu)$, where $I(0)$ is the incident intensity, $I(\nu)$ is the transmitted intensity, and $\sigma(\nu)$ is the absorption cross section.

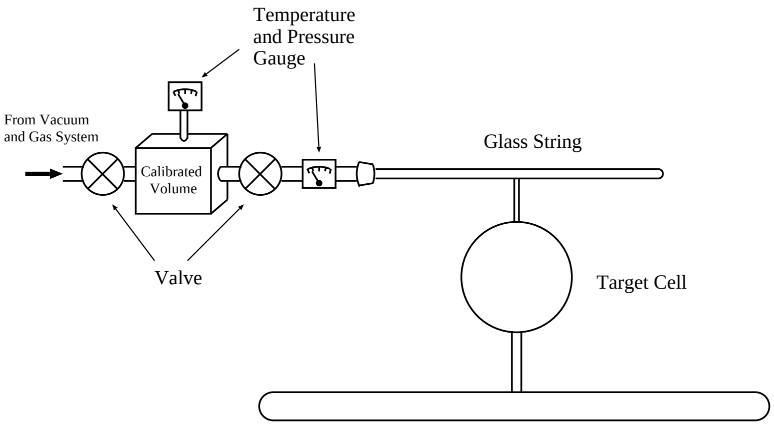

Figure 3.5: The cell filling system.

The absorption cross section has the form of an asymmetric Lorentzian:

$$\sigma(\nu) = \frac{A[1 + C \cdot \delta\nu]}{(\delta\nu)^2 + (\Gamma/2)^2} + B, \tag{3.10}$$

where A, B, and C are fit parameters and Γ is the line-width. Γ is proportional to the density of the gas: $n_0[\mathrm{cm}^{-3}]=\mathrm{k}_{broadening}\Gamma$. The constants of proportionality, $\mathrm{k}_{broadening}$, were determined using a reference cell filled to a known number density [61]. They are listed in Table 3.4. They are in units of Gigahertz per amagats. An amagat (amg.) is the number of particles per cubic centimeter at 0°C and 1 atmosphere: 1 amg. = 2.689×10^{19} cm^{-3}.

	^{3}He	N_2
D1 full width [GHz/amg]	18.7±0.3	17.8±0.3
D2 full width [GHz/amg]	20.8±0.2	18.1±0.3

Table 3.4: Constant of proportionality used to determine density from optical line broadening.

For each cell both the fill density and the average of D1 and D2 line widths were recorded. The average of the D1 and D2 results are considered one measurement of the ^{3}He density. The uncertainty in this method is 1.1%. The results are listed in

Table 3.5. Results of the measurements, along with a weighted average, are listed in Table 3.5. The uncertainty on the final weighted average of the density is assigned to be ±1.0%.

Cell	D1	D2	D1-D2 Ave.	Fill	Weighted Mean (n_o)
Don't Worry	10.03	9.94	9.99	9.82	9.93
Be Happy	9.28	9.39	9.34	9.33	9.32
Armageddon	10.09	10.25	10.17	10.14	10.15
Nepheli	11.47	11.32	11.40	11.0	11.33
Sysiphos	8.31	8.14	8.23	8.09	8.16
Jin	8.46	8.42	8.44	8.42	8.41

Table 3.5: Results of measurements of the ^{3}He density in amagats.

3.3 Target Setup

The target used for the E94-010 experiment is comprised of three main systems: an optical pumping system, a Nuclear Magnetic Resonance (NMR) system used to measure the target's polarization, and an Electron Paramagnetic Resonance (EPR) system, discussed in Section 4.2.8, used to calibrate the NMR system (Figure 3.6).

Optical Pumping System

The optical pumping system's principal components are the Helmholtz coils used to create a holding field and the laser system used to optically pump the rubidium's outer shell electron. Two sets of Helmholtz coils were to used create a uniform field of 20 Gauss about the target. The two coil sets were perpendicular to one another and turned 19 degrees off of the central beam line (Figure 3.7). Their approximate size was 60 inches in diameter (Figure 3.8). The direction of the holding field was kept along the beam path and rotated perpendicular to the beam in order to redirect the ^{3}He spins.

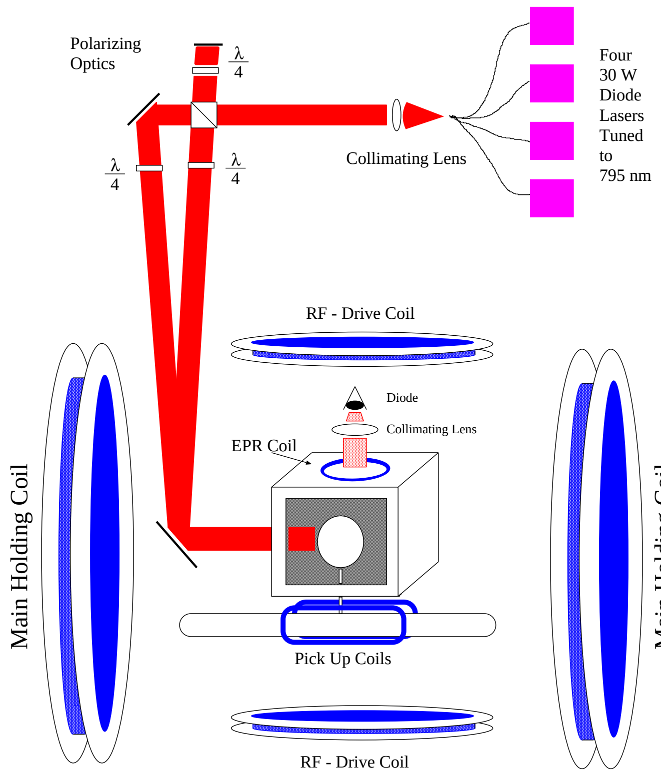

Figure 3.6: Schematic of the E94-010 target showing components of the pumping system, NMR system, and EPR system. A second set of Helmholtz coils is not shown.

The laser system used to pump the rubidium vapor was designed and constructed at Caltech (Figure 3.9). Its basic structure is comprised of seven diode lasers, a set of circular polarizing optics to polarize the laser light, and a set of mirrors and lenses to direct the light towards the target. The entire system was housed in a protective concrete hut located near the target on the Hall A floor. The diodes were manufactured by *OptoPower*. They consist of two 15 Watt diode bundles that are coupled together into one fiber optic cable. The lasers have both local current and temperature controls, and a system was created that allowed for control of the laser operation from the counting house. The output had a FWHM of $\leq$2.5 nm and achieved 30 Watts of output power at a central wavelength of 795 nm. The light that is emitted from the end of the fiber optic cable comes out in a 12° cone.

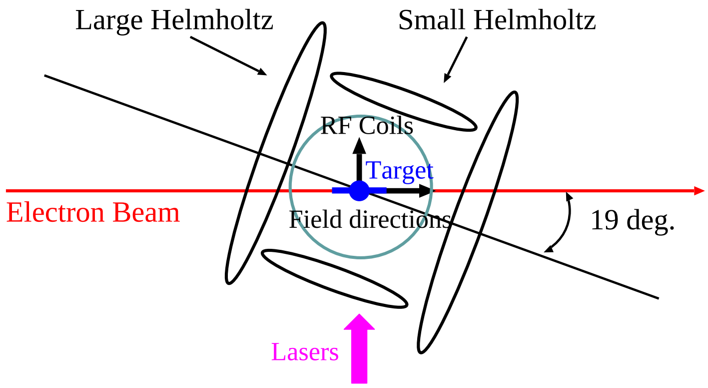

Figure 3.7: A top view of the E94-010 target.

The system of optics (Figure 3.9) used to direct the divergent diode laser to the target starts with a collimating lens. Using a polarizing cube, the light is split into its S and P components of linear polarization. The P component passes straight through the cube and reflects off a mirror. It then passes through a quarter-waveplate and on towards the target. The S component passes out of the polarizing cube at 90°. Moving away from the target, the S component passes through a quarter-waveplate, is reflected by a mirror, and back through the same quarter-waveplate. This process has the effect of rotating the sense of polarization by 90°. The light then passes straight through the polarizing cube and then through a quarter-waveplate on its way towards the target. Four of the seven lasers were dedicated for pumping in the longitudinal direction (when the magnetic field is aligned with the electron beam). Once the light from these lasers reach the target area, they are directed down and onto the target by a pair of compensating mirrors. The other three lasers are used for transverse pumping (when the magnetic field is pointing 90° with respect to the electron beam direction) and reach the target directly from the side. Helicity of the longitudinal lasers could be reversed remotely using a set of half waveplates. The laser system was robust and ran with nearly 100% efficiency during the experiment.

The ^{3}He target was mounted to a target ladder which also contained spaces for a reference target and a carbon foil target (Figure 3.10). The reference target could

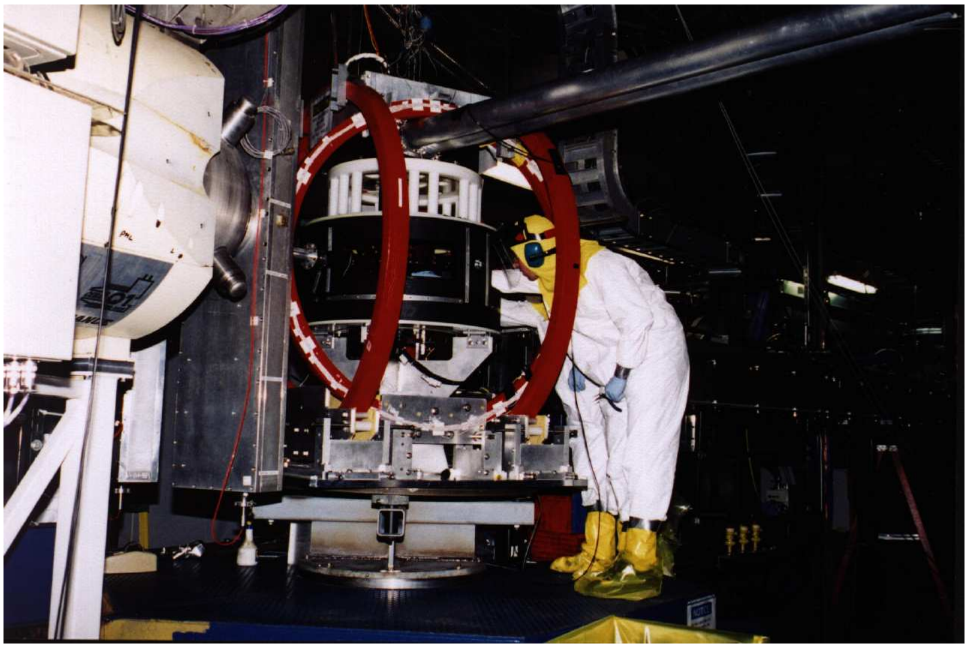

Figure 3.8: The E94-010 target in situ at Jefferson Lab.

be evacuated or filled with either N_2 or ^{3}He up to 70 psi. The carbon foil target had seven thin plates of carbon spaced evenly apart. It was used to study the optics of the spectrometers. Finally, the target could be put into a “no-target” position for beam tuning.

The target ladder was mounted onto a Torlon (a high temperature plastic) oven which was used to heat the pumping chamber. Hot air was passed into the oven through an electric coil heater. The temperature was regulated using a Resistive Thermal-couple Device (RTD) mounted on the inside of the oven. The oven was mounted to a rod that could move vertically, allowing the different targets into the beam line remotely. Cooling jets of ^{4}He were directed at the end windows of the target chamber to cool them from the electron beam heating.

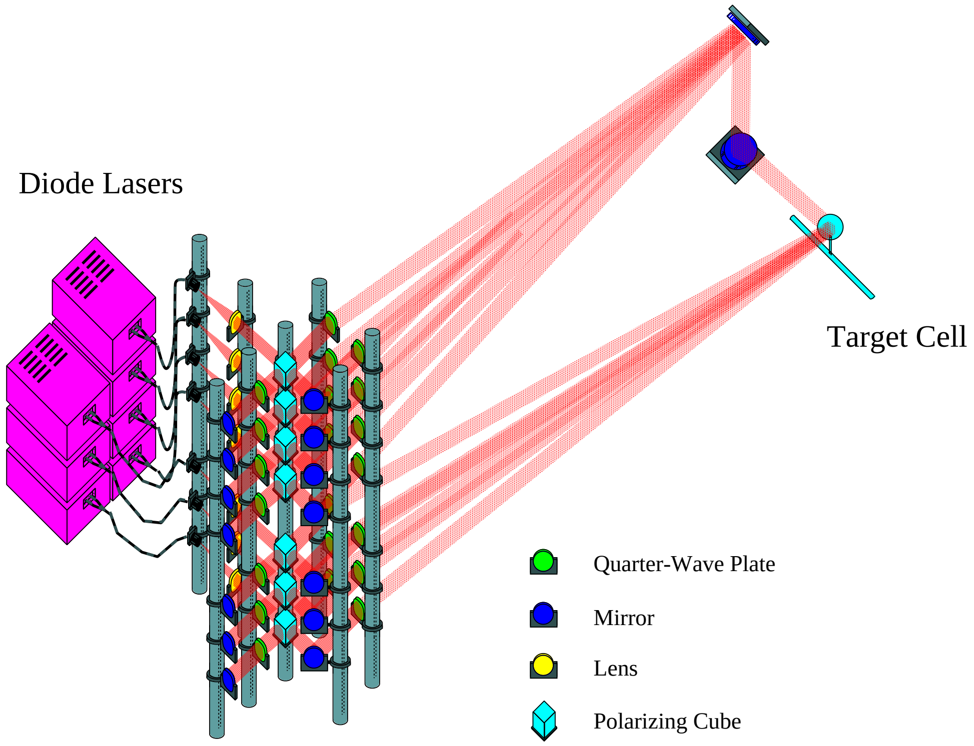

Figure 3.9: The E94-010 laser system. Not shown in the drawing is a set of half-waveplates that could be moved in and out of the laser path to reverse the helicity.

NMR System

The value of the ^{3}He polarization was determined from observing the ^{3}He Nuclear Magnetic Resonance (NMR) signal. Two additional components were added to the system in order to make this measurement (Figure 3.6). A Helmholtz coil was placed around the target in order to create a vertical RF field. The field had a frequency of 91 kHz and a magnitude of about 100 mG. A set of pickup coils was placed within the target chamber and used to detect the NMR signal. They were 1 inch tall, 4 inches long, and 1/2 inch wide. Each coil had 150 windings of 32 gauge copper wire. When a measurement needed to be taken, the target chamber was lowered out of the beam path and placed in between the pick coils (Figure 4.4).

The NMR system was controlled using a computer located in the counting house (Figure 3.11). The signal from the pickup coils was read by a lock-in amplifier refer-

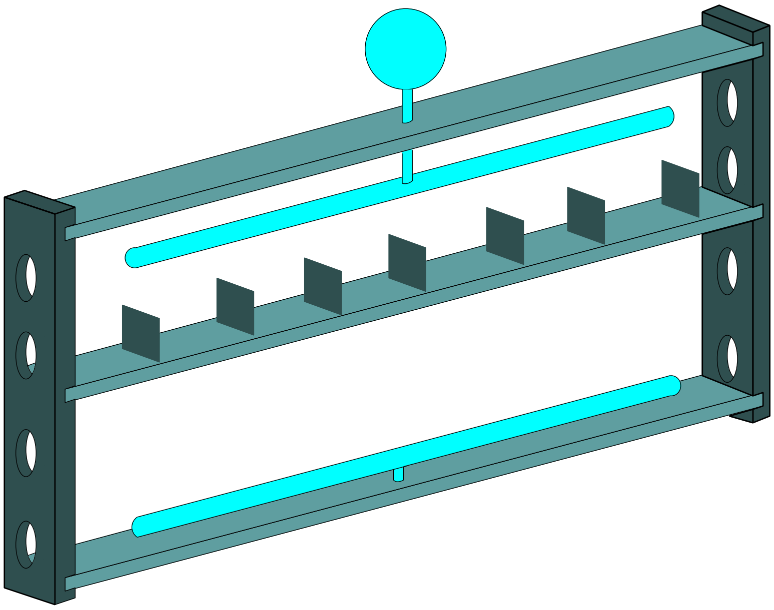

Figure 3.10: The target ladder used for the E94-010 experiment. The ^{3}He, reference, and carbon targets are shown.

enced to a RF generator. The output of the RF generator went into a RF amplifier located in the counting house, which was then connected to the RF coils located in Hall A. The magnitude of the holding field was swept from 18 to 25 Gauss using a function generator. The function generator creates a voltage sweep that is fed into the control input of a Kepco power supply.

3.3.1 Cell Temperature

Heating the pumping chamber causes ^{3}He to concentrate in the target chamber in order to equilibrate the pressure throughout the cell. Assuming an ideal gas law, the relation of the number density for a particular chamber to the nominal density is given by:

$$\frac{n_p}{n_0} = \left(1 + \frac{V_{target}}{V_{total}}\left(\frac{T_p}{T_t} - 1\right)\right)^{-1} \quad \text{and} \quad \frac{n_t}{n_0} = \left(1 + \frac{V_{pump}}{V_{total}}\left(\frac{T_t}{T_p} - 1\right)\right)^{-1}. \tag{3.11}$$

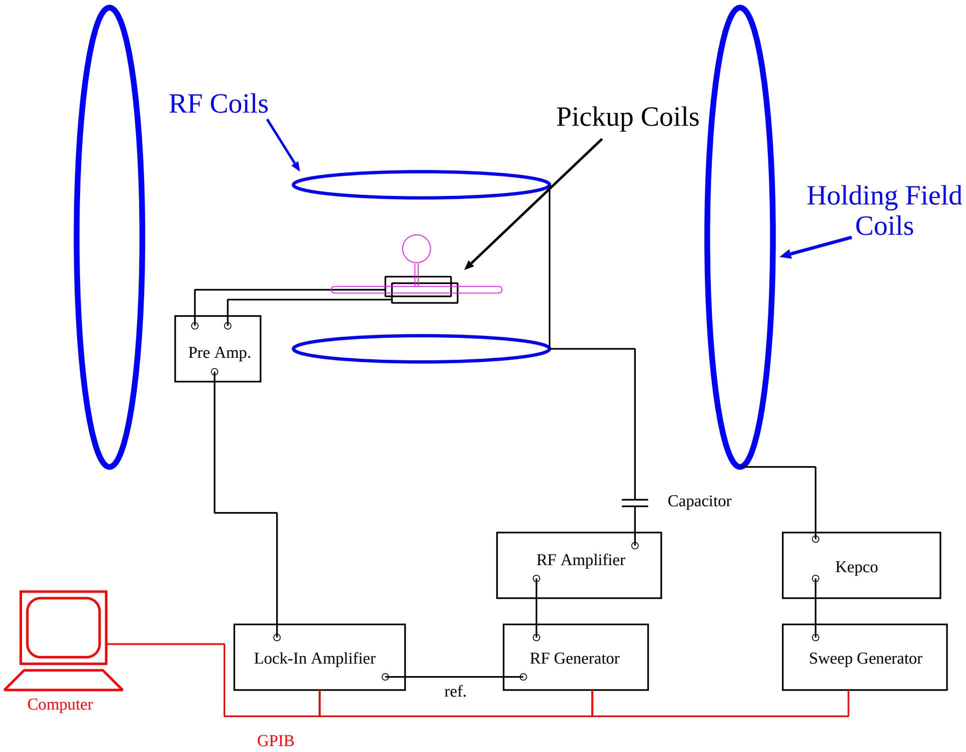

Figure 3.11: Schematic of the electronics used in the NMR system.

Here $n_{p(t)}$ and $T_{p(t)}$ are the volume averaged number density and temperature for the pumping (target) chamber. The volumes–V_{total}, V_{target}, and V_{pump}– are listed in Table 3.3 and the nominal densities, n_0, are listed in Table 3.5. What is needed to calculate $n_{p(t)}$ are the chamber temperatures.

In order to understand the temperature distribution each cell used had seven resistive thermocouple devices (RTDs) attached to them: two RTDs placed on the pumping chamber and five RTDs placed along the target chamber separated by 6 ± 1 cm (Figure 3.12). The RTD values were recorded by hand before polarimetry measurements were performed and by the DAQ at the beginning of each data taking run. At room temperature the RTD readings did not differ by more than 1°C. Under running conditions, the relative RTD readings were stable to within a few degrees. Average RTD values were calculated from all the values (75 to 150) recorded for a particular cell. To this value 1.4°C, as determined from a previous study [50], was added to reflect a slight drop in temperature across the cell wall. The standard deviation on this average was approximately 3.5°C, and an uncertainty of 5°C was placed on each average RTD value.

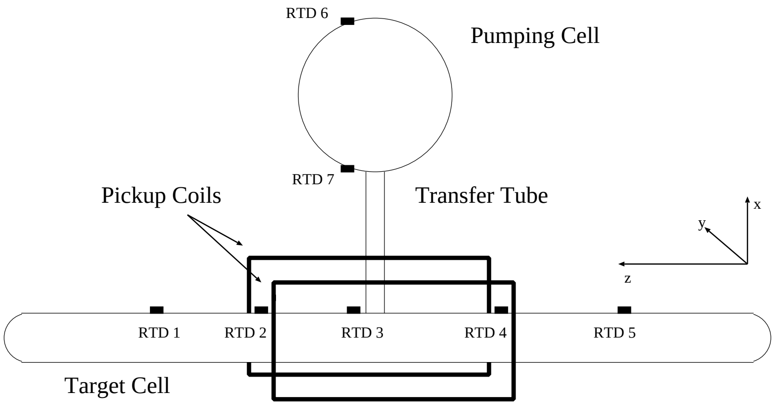

Figure 3.12: Position of the RTDs used to measure the temperature of a target cell.

A weighted sum of the RTD values was used to calculate T_t:

$$T_t = (6/40)(\mathrm{RTD}\#2 + \mathrm{RTD}\#3 + \mathrm{RTD}\#4) + (11/40)(\mathrm{RTD}\#1 + \mathrm{RTD}\#5). \quad (3.12)$$

Measurement of the pumping chamber's volume averaged temperature, T_p, is complicated by the deposition of heat from the lasers. Since the lasers tend to heat the center of the chamber, the temperature difference between T_p and the average of the pumping chamber RTDs ($\frac{1}{2}(\mathrm{RTD}\#6 + \mathrm{RTD}\#7)$) can be quite large. By looking at cases where two NMR signals, one with lasers on and one with lasers off, were conducted closely in time with one another, a prediction for this difference can be made.

The strength of a NMR signal is proportional to the density of ^{3}He between the pickup coils: $n_c = n_t(T_t/T_c)$, where T_c=(1/2)r3+(1/4)(r2+r4) is the temperature of the gas between the coils. If a NMR signal is obtained when the lasers are on (S^{on}_{He}) and when they are off (S^{off}_{He}), the temperature of the pumping cell while the lasers were on is given by:

$$T_{predicted} = \frac{V_{pump} T_t^{on}}{\frac{S_{He}^{off}}{S_{He}^{on}} \frac{T_t^{on} T_c^{off}}{T_t^{off} T_c^{on}} \left[V_{total} + V_{pump} \left(\frac{T_t^{on}}{T_p^{off}} - 1 \right) \right] - V_{total} + V_{pump}} \tag{3.13}$$

Equation 3.13 is predicated on the assumption that all RTD measurements truly reflect the temperature inside the cell, except those on the pumping chamber when the lasers were on.

During the experiment there were 17 cases where a NMR measurement was performed with the lasers in one state and 5 to 15 minutes later with the lasers in the other state. The amount by which the pumping chamber is hotter than the average of RTDs #6 and #7 is called Δ. The 17 values calculated for Δ are shown in Figure 3.13. There was a large range of values predicted for the interior pumping chamber temperature with seemingly no correlation to the amount of time between NMR measurements or to whether the lasers were on or off initially. The large variation in results is most likely from unrecorded conditions at the time of the measurement.

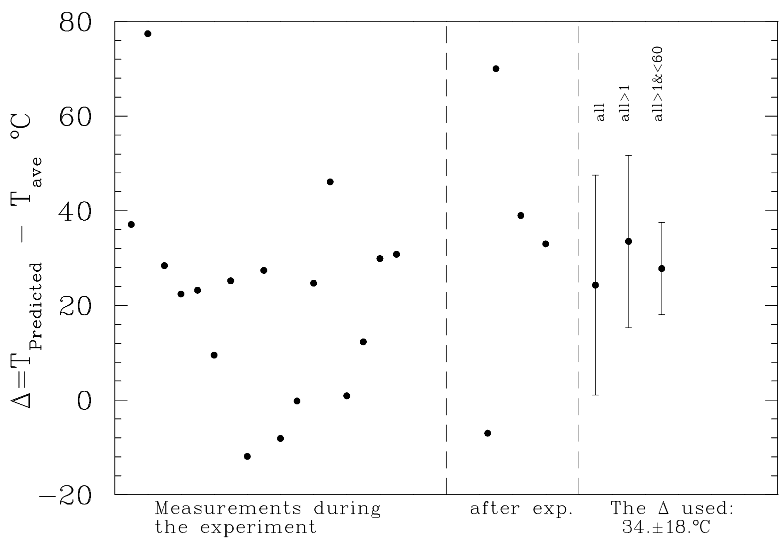

Figure 3.13: Measurements of Δ. Errors bars are standard deviations for different data sets.

To understand the variations, four, carefully recorded tests were conducted after

Cell	T_p (°C)	T_c (°C)	T_t (°C)	n_p/n_0	n_t/n_0	n_c/n_0
Don't Worry	235	67	64	0.825	1.224	1.211
Be Happy	221	57	53	0.829	1.234	1.221
Armageddon	213	62	54	0.819	1.201	1.175
Nepheli	214	57	55	0.821	1.201	1.194
Sysiphos	213	53	51	0.815	1.207	1.201
Jin	220	59	53	0.824	1.208	1.188

Table 3.6: Temperatures and relative densities.

the experimental run (Figure 3.13). The negative prediction for Δ was correlated to heaters coming on at the same time the lasers were turned off. This had the effect of temporarily making the pumping chamber hotter and forcing more ^{3}He into the target chamber. To circumvent this effect, two of the tests were done with both the laser and heater turned off. The calculated results for Δ were 39 and 34°C. The fourth test attempted to reproduce the conditions of the measurements taken during the experimental run. This time Δ was equal to 71°C. There was no apparent reason for this high value.

An average of all the measurements, which had a value greater than one, was used to calculate Δ. The uncertainty applied to this number was the standard deviation of these points. The final result of Δ was 34±18°C and $T_p = \Delta + (1/2)(\mathrm{r6} + \mathrm{r7})$ with an assigned uncertainty of ±18°C.

Using the results for T_p, T_t, and the volumes, Eqs 3.11 were solved. The results are listed in Table 3.6. Each relative density has an uncertainty of ±2.0%.